Cracking Susceptibility of Ti-6Al-2Nb-1Ta-0.8Mo as Determined by the Varestraint Test

Cracking susceptibility was reduced by altering phase transformation

BY D. HAYDUK, B. K. DAMKROGER, G. R. EDWARDS AND D. L. OLSON

ABSTRACT. Autogenous GTA welds have been made on the titanium alloy Ti-6Al-2Nb-1Ta-0.8Mo in an environmental chamber containing a Varestraint testing fixture. The cracking susceptibility of Ti-6211 was investigated and compared with that of Ti-6Al-4V. No cracking was seen in the alloy Ti-64. However, sub-solidus cracking was observed in both the fusion zone and the heat-affected zone of Ti-6211 welds made using a wide variety of process variables. This cracking was intergranular at prior-beta grain boundaries and oriented perpendicular to the axis of applied strain. The strain sensitivity of Ti-6211 was investigated, and it was determined that between 1% and 2% augmented strain was required to induce cracking.

Thermal analysis was used to obtain the cracking temperature range for each weld. These critical temperatures were found to lie within the beta-to-alpha transformation. This was interpreted as indicating that the cracking is related to the solid-state phase transformation. Parallel observations in both weld cracking Varestraint tests and hot ductility tests in Ti-6211 indicate that these are different manifestations of the same phenomena.

Introduction

The titanium alloy Ti-6Al-2Nb-1Ta-0.8Mo, or Ti-6211, is considered promising as a structural material for marine applications, due to its excellent stress corrosion cracking resistance, high specific strength, and good fracture toughness. Fabrication of this alloy typically involves elevated temperature processing techniques, including welding, forging, and hot rolling. A particularly critical requirement for the use of this material in structural applications is good weldability. Although solidification and liquation cracking have been observed in titanium alloys, these alloys generally are considered to have excellent weldability, with little susceptibility to this type of cracking (Refs. 1–3). The relatively low partitioning ratios for the alloying elements in Ti-6211 should make this alloy similarly resistant to these cracking problems (Refs. 4, 5).

Although not susceptible to liquation cracking, previous studies (Refs. 6–9) have indicated that Ti-6211 is susceptible to a severe loss in ductility at elevated temperatures. This ductility loss occurs on cooling in thermal cycles characteristic of fusion welding. Also, during high-temperature fabrication operations, Ti-6211 has been shown to be susceptible to intergranular cracking at the beta grain boundaries (Ref. 9). Transgranular and intergranular cracking have also been observed in the fusion zone of highly constrained multiple-pass welds (Ref. 8). The conditions common to all of these processes are thermal cycling to a temperature above the beta transus, followed by the application of a tensile strain, upon cooling, at a temperature near the beta-to-alpha transformation temperature.

Lewis and Caplan (Ref. 6) tested Ti-6211 and several titanium alloys for susceptibility to hot ductility losses. In this study, a programmable thermomechanical testing device (Gleeble) was employed to investigate the hot ductility of commercial purity titanium Ti-6Al, Ti-3Al-2.5Sn, Ti-6Al-4V, and Ti-6211. Samples were subjected to a thermal cycle typical of a near-HAZ position in a GTA weld, and tensile tested at several temperatures on cooling. The unalloyed titanium and Ti-3Al-2.5Sn showed little or no loss of high-temperature ductility. Ti-6Al and Ti-6Al-4V did, however, exhibit a moderate hot ductility loss, though not as severe as Ti-6211 (Ref. 6). In an earlier study by Savage and Lundin (Ref. 2), two titanium alloys, Ti-6Al-4V and Ti-3Al-14V-11Cr, were tested for hot cracking using the Varestraint test. Liquation cracking was observed in Ti-3Al-14V-11Cr, but no sub-solidus cracking was reported in either alloy. Earlier work by the authors showed that three near-alpha titanium alloys, Ti-6Al-2V-2Zr, Ti-6Al-2V-4Zr, and Ti-6Al-2V-6Zr, were highly resistant to elevated temperature weldment cracking (Ref. 7).

Several investigators have studied the metallurgical factors associated with the hot ductility losses observed in Ti-6211 (Refs. 6–10). Macroscopically, the failures were observed to occur intergranularly along prior-beta grain boundaries and with very little ductility. However, scanning electron microscopy revealed ductile dimpling on the grain surfaces, indicating that failures occurred by microvoid nucleation and coalescence (Refs. 7, 9). Examination of the fracture surfaces did not reveal second-phase precipitates. Microprobe and Auger electron analysis of both the fracture surfaces and prior-beta grain boundaries also failed to reveal any significant elemental concentration. These results differ from those made in related investigations. Lewis (Ref. 6) found a sulfur concentration of over three-hundred times the bulk concentration on the fracture surface of Ti-6211 specimens which were thermally cycled and fractured at room temperature and 77 K. Also, in a weldability study of Ti-6211, David found that weldments made with filler metal wire containing boron had low room temperature impact

Based on a paper presented at the 64th Annual AWS Convention, held April 24–29, 1983, in Philadelphia, Pa.

D. HAYDUK, B. K. DAMKROGER, G. R. EDWARDS and D. L. OLSON are with the Center for Welding Research, Colorado School of Mines, Golden, Colo.

Table 1—Chemical Composition of Ti-6211 Base Material (wt-%)

Al	Nb	Ta	Mo	Fe	C	N	O	H[a]
6.0	1.9	0.90	0.81	0.09	0.02	0.009	0.071	52

[a]Parts per million.

toughness (Ref. 10). In this study, microanalysis revealed boron-rich precipitates along grain boundaries. It was not determined whether the reduced impact toughness occurred as a result of the grain boundary precipitates.

The alloy Ti-6Al-4V, the most commonly used of the structural titanium alloys, has also been investigated with respect to the ductility losses (Refs. 6–8). Though this alloy did undergo a moderate loss of hot ductility as previously mentioned, Ti-6Al-4V is generally considered to have excellent weldability and to be free from weld cracking problems. Ti-6Al-4V will be used as a reference in this study.

Objectives

The objectives of the present study were as follows:

1. To investigate the presence of high-temperature ductility losses in Ti-6211 weldments.
2. To evaluate the influence of welding process variables on the cracking susceptibility of Ti-6211.
3. To metallurgically characterize the cracking in Ti-6211 weldments.
4. To isolate and identify the mechanism responsible for weld cracking in Ti-6211.
5. To investigate the effects of the interstitial elements oxygen and nitrogen on the Varestraint cracking susceptibility of Ti-6211.

Experimental Procedure

The Ti-6211 used in this study was 0.5-in. (12.7-mm) thick, beta-processed (cross-rolled in the beta phase field) plate. The chemical composition of the material is given in Table 1.

Varestraint-Equipped Welding Chambers

Stainless steel, protective atmosphere glove boxes were equipped with the necessary apparatus for the combined welding and Varestraint testing programs. The GTA welding was carried out with a water-cooled torch, using direct current, electrode negative connections. All GTA welds made in this investigation were autogenous bead-on-plate welds. Both current and travel speed were varied to give nominal GTAW heat inputs ranging from 10 to 60 kJ/in. (0.4 to 2.4 MJ/m). The GMA welds were made using a variable slope power supply and electrode negative connections. A remotely controlled programmable wire feed system was employed, and either 0.030- or 0.045-in. (0.76- or 1.14-mm) diameter wire. The GMA weld variables were chosen to produce constant deposition rates of 0.030 and 0.040 in.^{3}/in. (19.4 and 25.8 mm^3/mm) and a constant heat input of 22 kJ/in. (0.8 MJ/m). The argon atmospheres in both chambers were periodically monitored by gas chromatography. Sample color was used as an additional check for atmospheric contamination (Ref. 1). Prior to testing, the titanium specimens and the steel backing bars were degreased with acetone.

The simplified sketch of the Varestraint system (Fig. 1) shows the fundamental operation of this test (Ref. 11). The specimen is supported as a cantilever beam and deformed by a hydraulically actuated clevis, as the weld is being made. The Varestraint system is actuated when the welding torch reaches the tangent point of the strain mandrel. The sample is deformed to the shape of the strain mandrel, putting the desired augmented strain in the top surface of the weldment. The welding torch is allowed to continue to the end of its travel, approximately 1.5 in. (40 mm) beyond the tangent point, before being extinguished. After the arc is extinguished, the load is sustained for approximately one minute. Interchangeable strain mandrels are used to give augmented strains of ½%, 1%, 2%, and 4% longitudinal tensile strain.

Specimen Examination

Metallographic specimens were prepared using standard techniques. The etchant used was a 2½% HF, 5% HNO_3, aqueous solution applied for approximately 5–10 s.

The fracture surfaces of the Varestraint tested weldments were examined using scanning electron microscopy. The weld cracks were opened by cutting through the weldment to the crack tips with a diamond wafering saw and then pulling the section apart. The fracture surfaces were ultrasonically cleaned in acetone, and no surface preparation was used.

A 15×–60× stereomicroscope was used to identify and quantify the extent of cracking in the Varestraint samples. Oblique, high-intensity lighting was used to help identify the less conspicuous cracks. The length of each crack and the distance from the crack to molten weld pool position at the instant of straining were measured. The molten weld pool position at the instant of straining was indicated by a slight disturbance of the weld bead.

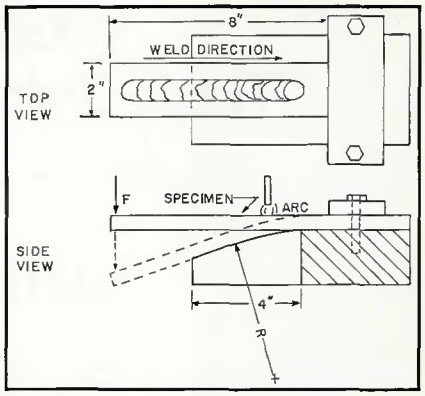

Fig. 1—Schematic diagram of Varestraint test apparatus and operation

Thermal Analysis

The thermal analysis technique used in this investigation was similar to one used previously by Savage and Lundin (Ref. 13), and is shown schematically in Fig. 2. Calibrated tungsten-rhenium thermocouples were used for the thermal analysis of Ti-6211 weldments. Welds were made on specimens of the same geometry as the Varestraint specimens, and identical fixturing was used so as to accurately reproduce the cooling conditions present during Varestraint testing. During welding, the thermocouple was manually plunged into the molten weld pool immediately behind the arc and became permanently fixed in the weld pool as the weld solidified. A strip-chart recorder was used to collect the output of the thermocouple, resulting in a record of the thermal profile of the weldment during cooling. These cooling curves were used in conjunction with the Varestraint test measurements to determine the temperature range of cracking. In the GTA weldments, the distance from the trailing edge of the weld pool during straining to the location of fusion zone cracking was taken from Fig. 10. The distance was converted to a time interval, using the torch travel speed for each weldment. The assumption was then made that the cracking occurred at the instant the Varestraint strain was applied. This resulted in the calculated time interval being equivalent to the time for the weld metal to cool from the liquidus temperature, 2800°F (1540°C), to the critical cracking temperature. A similar technique was used for the fusion line cracking in the GMA welds. In this case, the distance to the position of cracking was measured from the corresponding position of the

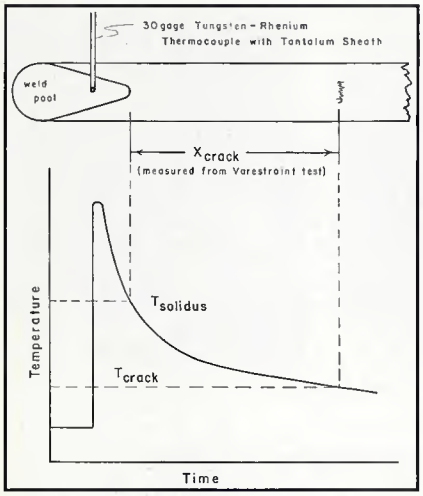

Fig. 2—Thermocouple harpoon and thermal analysis technique

molten pool at the time of strain application.

Deliberate Interstitial Contamination

The deliberate contamination of the weld metal with either oxygen or nitrogen was accomplished through additions to the argon torch gas. Various argon-contaminant mixtures were made and analyzed, using gas chromatography before welding. Following welding, the weld metal interstitial concentrations were measured.

Results and Discussion

GTAW Varestraint Testing

Preliminary Varestraint testing was done on test specimens of both Ti-6211 and Ti-6Al-4V using a moderate heat input, 33 kJ/in. (1.3 MJ/m), and the maximum augmented strain possible, 4%. The alloy Ti-64 showed no tendency to crack at any point in either the weld metal or the heat-affected zone. However, cracking was observed in both the fusion zone and the heat-affected zone of the Ti-6211 weldments. Macrographs of the top surface of one of these weldments (Fig. 3) illustrate this cracking. The direction of arc travel in these macrographs is from right to left. The cracks follow the large prior-beta grain boundaries and range in length from 0.02 to 0.1 in. (0.5 to 2.5 mm). All cracks are oriented perpendicular to the axis of the applied longitudinal strain, *i.e.*, perpendicular to the weld bead axis. Orientation of these cracks differs from the orientation of typical weld hot cracks, where the cracks are parallel to the weld axis (Ref. 3). No cracking was found immediately adjacent to the weld pool during straining, further indication that the cracking was not a typical hot cracking problem occurring near the liquidus temperature, but is occurring in a much lower temperature regime. The location of the molten weld pool at the instant of straining can be seen at the left edge of Fig. 3A. The cracking occurred in this weldment at locations 0.6 to 0.8 in. (15 to 20 mm) from the position of the weld pool during strain application.

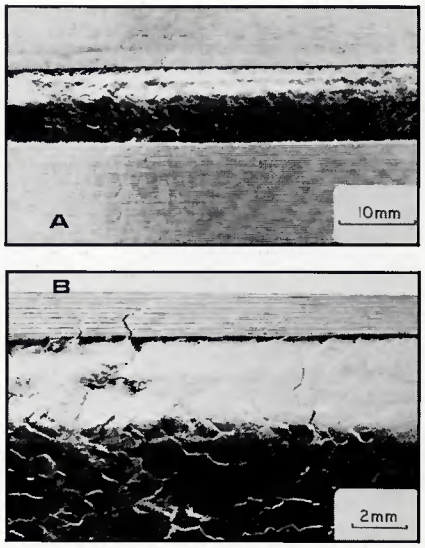

Fig. 3—Macrographs of Varestraint tested weldments showing intergranular cracking at the fusion line. The position of the molten weld pool at the instant of straining can be seen at the left edge of A

Fractography

Several of the Ti-6211 Varestraint weldments were sectioned and the cracks opened up to reveal the fracture surfaces for scanning electron microscopy. Figure 4 shows the fracture surface morphology of a fusion zone crack. The crack is oriented with the weld bead top surface at the top of the photo. The weld bead top surface can be seen in the low magnification photo. At this magnification, the large, columnar, prior-beta grains can also be seen, traversing the fusion zone. Inspection of this fracture surface shows it to be entirely intergranular along the prior-beta grain boundaries. At higher magnification, Fig. 4C, the surface is seen to be covered by ductile dimples, indicative of a ductile failure by microvoid nucleation and coalescence along the prior-beta grain boundaries. These characteristics suggest that a fine-alpha phase film, or other continuous second-phase film along the beta grain boundaries, may be responsible for this behavior. Evidence gathered by Lewis and other investigators support this possibility (Refs. 6, 7, 9). No evidence of grain boundary liquation can be seen in Fig. 4, further support for the presumption that this is a sub-solidus type of cracking.

Figure 5 is a similar series of SEM fractographs of a heat-affected zone crack. The specimen is oriented as in Fig. 4, with the weldment surface at the top of the photo. Although the prior-beta grains are equiaxed rather than columnar, the fracture morphology is nearly identical to that observed in the fusion zone. Again, the fracture is entirely intergranular and there is extensive ductile dimpling on the fracture surfaces. No evidence of second-phase particles or inclusions was found in either case.

Figure 6 is a set of optical micrographs of the FZ and HAZ in a Varestraint tested Ti-6211 weldment. These micrographs, taken at locations immediately adjacent to the cracks, show microstructures typical of an alpha-beta titanium alloy weld-

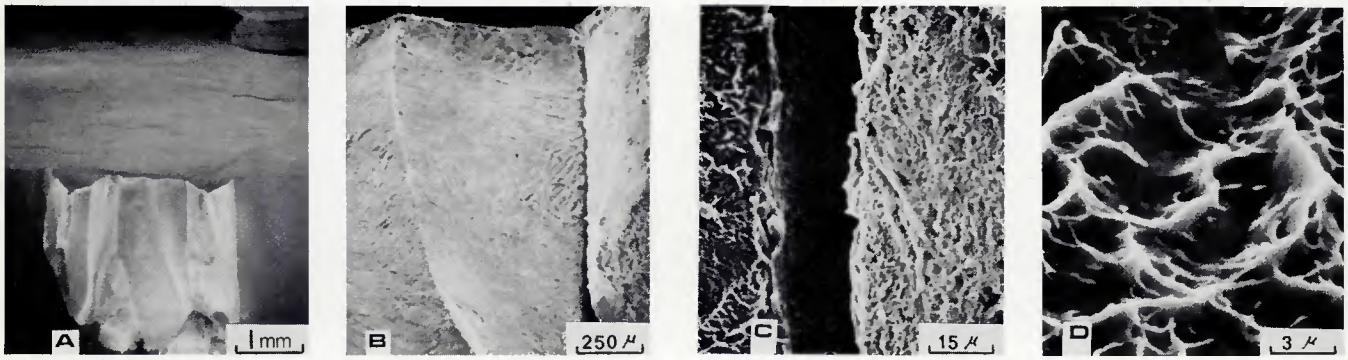

Fig. 4—Fractographs of an intergranular fusion zone crack showing that the failure occurs by ductile rupture of a grain boundary alpha film

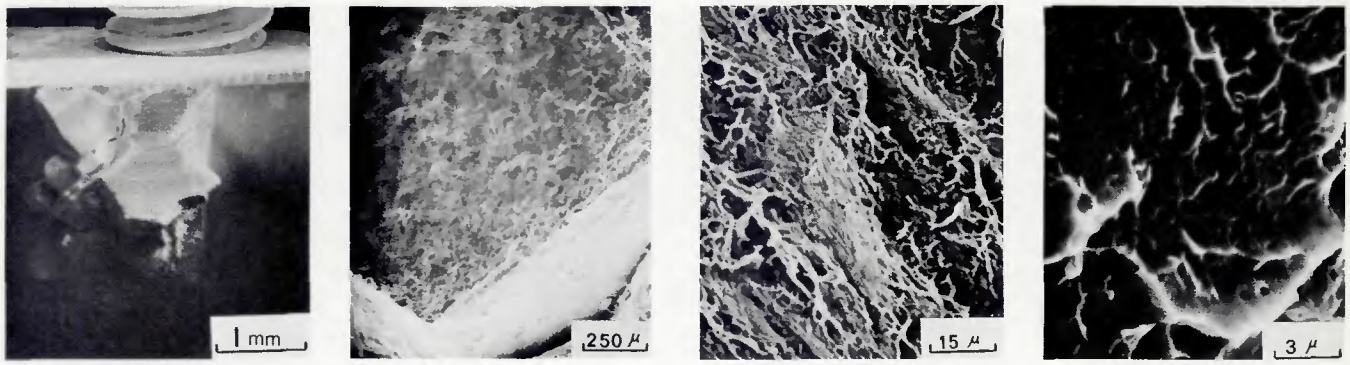

Fig. 5—Fractographs of a heat-affected zone crack. Note again that the failure, while macroscopically brittle, occurs by ductile rupture

ment (Ref. 12). The prior-beta grain boundaries are obvious, and the cracking follows these grain boundaries. The microstructure within the prior-beta grains consists of Widmanstatten alpha plus beta, and large, lenticular patches recently identified as either massive alpha or alpha-prime martensite (Ref. 14). A narrow grain boundary alpha film was found in most cases. An example of a grain boundary alpha film can be seen in Fig. 6A.

Figure 7 is a set of optical micrographs of the alloy Ti-64, Varestraint tested under the same conditions as the Ti-6211. Since the Varestraint test specimens of this alloy produced no cracking, these microstructures were taken at locations along the weldment where cracking was found in Ti-6211. The HAZ and FZ microstructures are both characterized by fine acicular alpha-prime martensite. The large, lenticular features seen in the Ti-6211 welds were not observed in Ti-64. A continuous grain boundary alpha film can be seen in these microstructures. This film is considerably thicker than that occurring in Ti-6211.

Characterization of Cracking

The Varestraint weld cracking was first characterized with respect to augmented strain level, using mandrels which provided 1%, 2%, and 4% augmented strain. Weldments were made at two heat inputs, 30 kJ/in. and 50 kJ/in. (1.2 MJ/m and 2.0 MJ/m), and tested at each level of augmented strain. The total crack length in each weldment was measured. These results are summarized in Fig. 8. While the amount of cracking was always less in the lower heat input weldment,

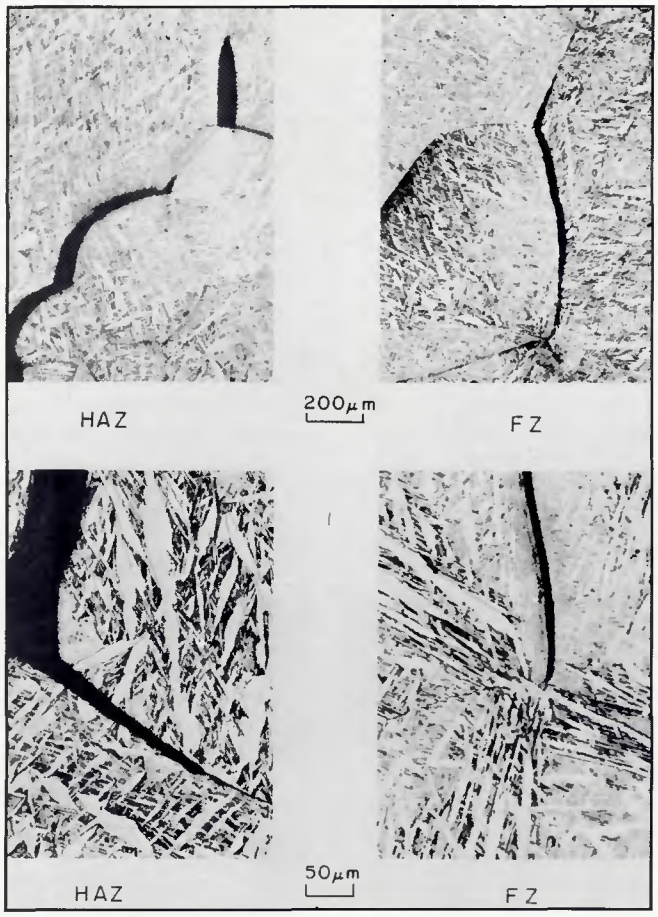

Fig. 6—Optical micrographs of cracked regions in the fusion zone and heat-affected zone

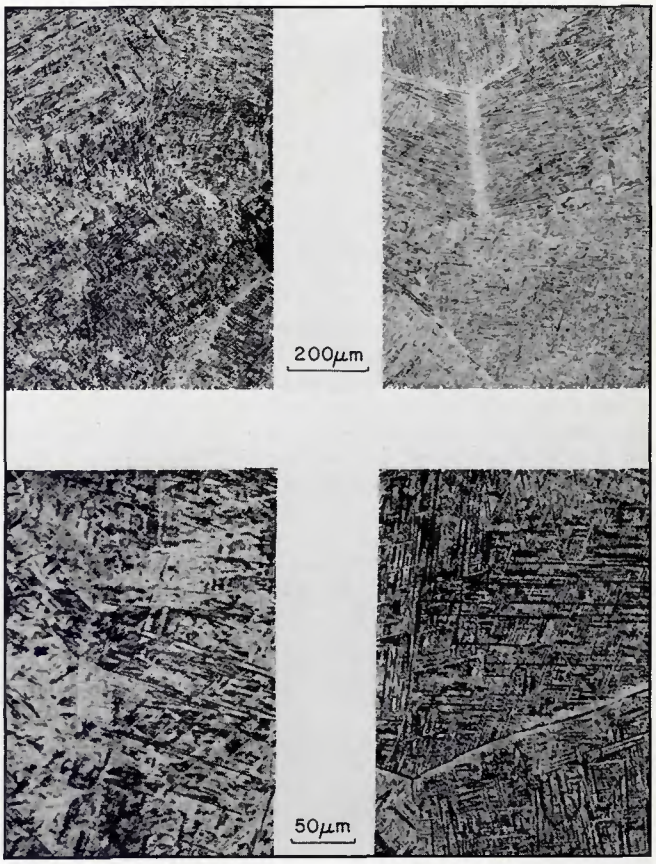

Fig. 7—Optical micrographs of fusion zone and heat-affected zone locations in a Varestraint tested Ti-64 autogenous single-pass GTA weldment. Note that this structure is much finer than that of Ti-6211, and does not contain the coarse, lenticular patches seen in Ti-6211

both heat inputs produced cracking at the 2% and the 4% strain levels. No cracking was observed in either heat input weldment at the 1% strain level. This implies that, in this test, a critical strain limit exists for Ti-6211 weldments between 1% and 2% augmented strain. Although the nature of the Varestraint test prevents a quantitative limit from being established, it is significant that a critical amount of strain is necessary for the cracking to occur.

The effect of GTA weld heat input on the cracking susceptibility of Ti-6211 was then investigated. Weldments were made using a range of heat inputs from 10 to 60 kJ/in. (0.4 to 2.4 MJ/m) and Varestraint tested at 4% augmented strain. The total lengths of both heat-affected zone and fusion zone cracks were measured at each heat input tested. These results are shown in Fig. 9. The first significant result was that all heat inputs used produced cracking, and that the extent of cracking increased with increasing heat input. The total amount of fusion zone cracking increased linearly with heat input, but the amount of heat-affected zone cracking remained approximately constant. This was explained by the observation that the fusion zone size increased with an increase in heat input, but the heat-affected zone size remained relatively constant.

A significant change was also noted in the position of the cracking as the heat input was varied. The distances from the weld pool position during straining to the cracks were measured as described in the experimental procedure. This was done separately for fusion zone cracks and heat-affected zone cracks. When more than one crack was found in either location, an average distance was reported. These measurements were taken for the entire range of heat inputs tested, and the results are given in Fig. 10. The heat-affected zone cracking was consistently located closer to the weld pool than the fusion zone cracking, as shown by the relative positions of the two curves. The measured distance increased linearly with increasing heat input for both the heat-affected zone and fusion zone cracking. These results show that the cracking phenomenon in Ti-6211 was related to the thermal experience of these weldments. The concentration of the cracking in a specific location suggests that the Varestraint cracking occurred over a narrow temperature range.

Further evidence that the cracking occurs over a narrow temperature range is given in Fig. 11. In this figure, the fusion zone and heat-affected zone cracks emanate from a teardrop-shaped halo. In a GTA welding process, this type of halo is believed to represent a 1500°F (815°C) isotherm (Ref. 15). On cooling, the beta-to-alpha transformation in Ti-6211 occurs

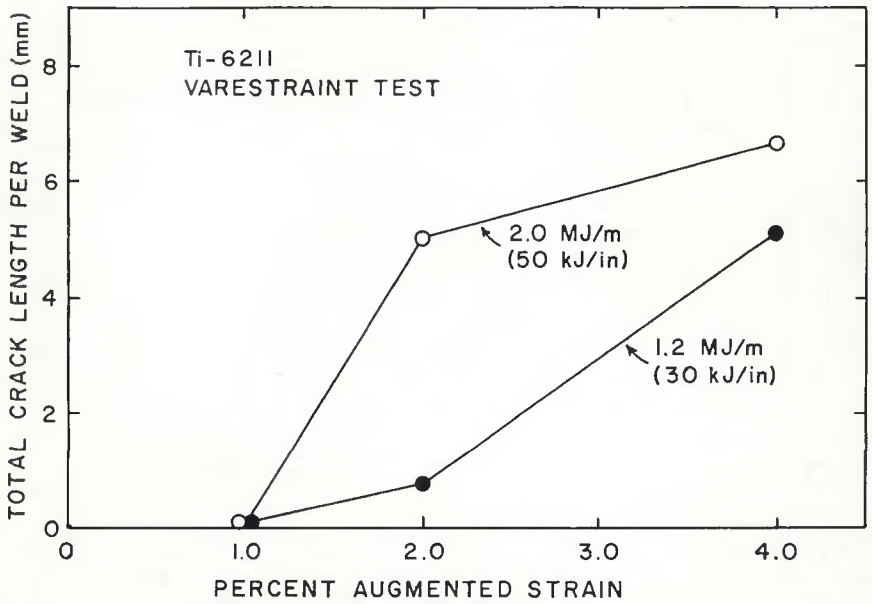

Fig. 8 — Total crack length per weld plotted as a function of percent augmented strain for two heat inputs

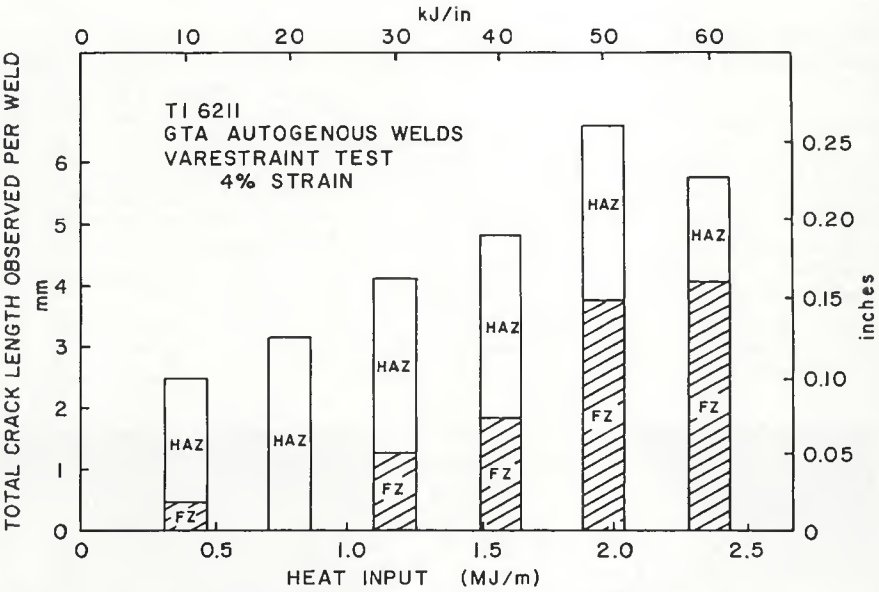

Fig. 9 — Fusion zone and heat-affected zone crack length versus heat input

at approximately 1600°F (870°C); consequently, the halo was interpreted as marking the position of the transformation zone at the instant of straining. The cracks near the halo imply that the cracking occurred within or near the transformation temperature range.

GMAW Varestraint Testing

Varestraint testing was performed on single- and multiple-pass GMA welds after one and three passes. A constant 20-kJ/in. (0.8-MJ/m) heat input was used. Augmented strains of less than 4% produced no cracking in Ti-6211, and no cracking was observed in Ti-6Al-4V control weldments, even at the 4% strain level. Cracking was observed in Ti-6211 at 4% augmented strain, after both one and three passes. In all cases, the cracking occurred at the fusion line of the last pass, but not at the crest of the last bead (where the augmented strain was greatest). Figure 12 shows the microstructures observed at the fusion line and bead crest of the last pass in a three pass GMA weld. The fusion line exhibited the coarse, lenticular microstructure previously shown to be susceptible to intergranular failure. In contrast, the bead crest exhibited a significantly more refined microstructure, reflecting the increased cooling rate experienced by

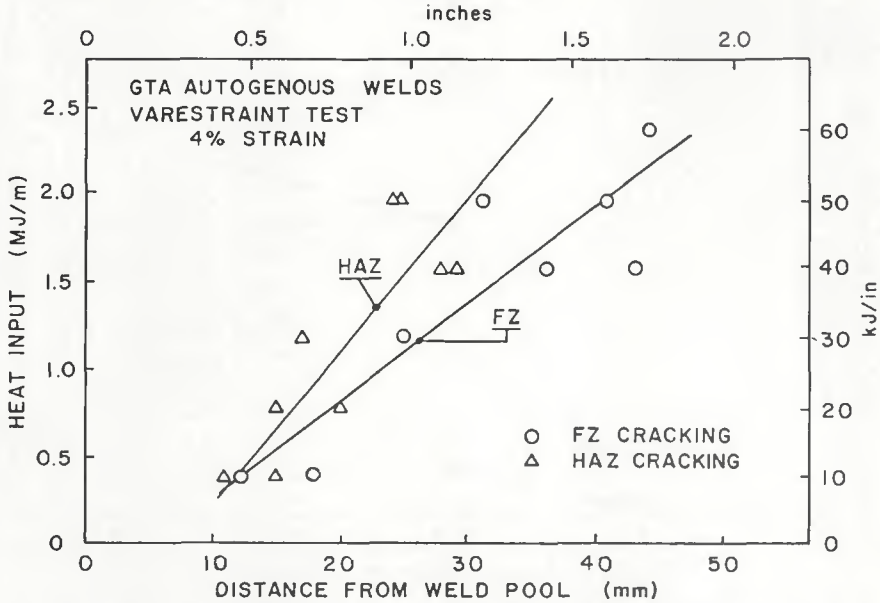

Fig. 10—Relationships between heat input, weld pool position at the instant of strain application and crack location

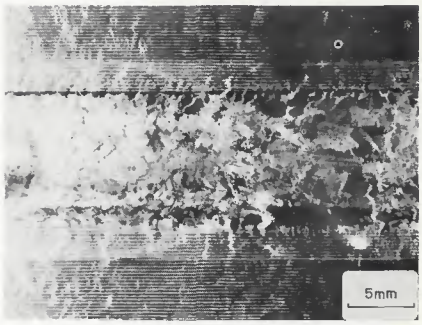

Fig. 11—Macrograph of a Varestraint tested weldment showing the cracking near a halo believed to mark the position of the beta-to-alpha transformation front at the instant of strain application

the crest. Both microstructures contain grain boundary alpha films.

Thermal Analysis

The temperature ranges of the Varestraint cracking were determined. These calculations utilized the thermal histories of the weldments and the positions of the Varestraint cracking as discussed earlier and shown in Fig. 2. The two cooling curves presented in Fig. 13 were obtained from GTA welds with heat inputs of 40 and 60 kJ/in. (1.6 and 2.4 MJ/m). When the calculated time intervals were superimposed onto the cooling curves, the temperature of cracking was determined for each weldment. The critical temperatures for the two welds were found to be 1365° and 1500°F (740° and 815°C), respectively. Also included in Fig. 13 are the reported liquidus temperature, 2800°F (1540°C), and the observed beta-to-alpha start temperature, approximately 1600°F (870°C).

When this analysis was repeated for five different weldments of varying heat inputs, the resultant cracking temperatures ranged from 1350° to 1550°F (725° to 850°C). The cooling curves for all of these weldments were plotted on the Ti-6211 continuous cooling diagrams of Gordine (Ref. 16) and Damkroger (Ref. 7), shown in Fig. 14. Both the critical cracking temperature and the recalescence temperature are shown for each cooling curve. Three important observations can be made with respect to this figure. First, the beta-to-alpha start temperatures seen in this investigation are consistent with the temperatures reported by Gordine and Damkroger (Refs. 7, 16). Second, the cracking temperature decreases with higher cooling rates. The third observation is that the cracking temperatures are associated with the beta-to-alpha transformation and appear to fall within the transformation. This is consistent with the observation of cracking near the transformation halo, shown in Fig. 10. It is believed that this preliminary evidence suggests that the cracking phenomenon is related to the solid-state transformation.

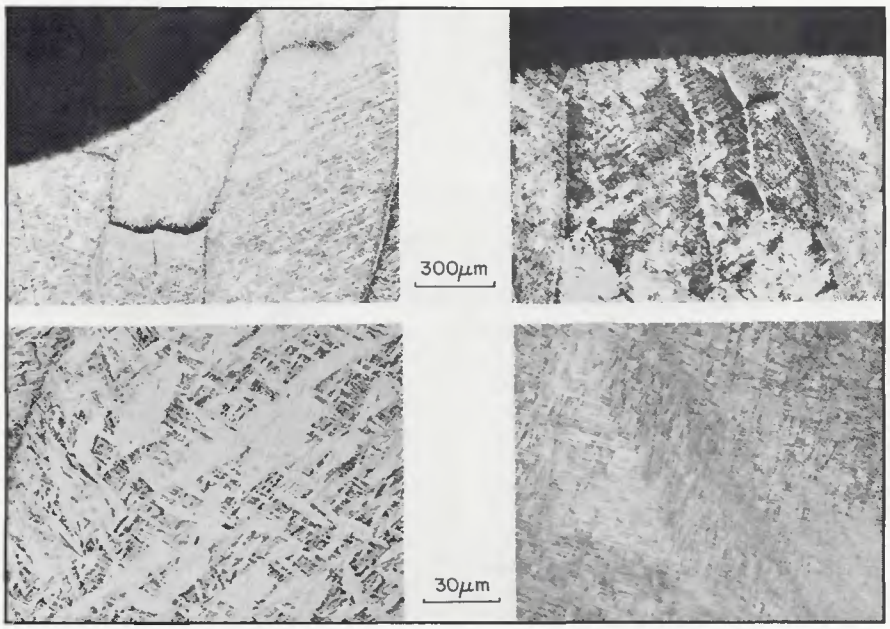

Fig. 12—Optical micrographs of the fusion line and bead crest of the last pass of a three-pass GMA weldment in Ti-6211. Note that the microstructure at the bead crest is much finer than that seen at the fusion line

Interstitial Contamination of GTA Weldments

The effect of atmospheric surface contamination on the Varestraint cracking susceptibility of Ti-6211 GTA weldments was studied. The two contaminants investigated were oxygen and nitrogen. Welds were made with shielding gas compositions consisting of 0.5 to 5.0% oxygen or nitrogen in argon. Figure 15 shows these shielding gas compositions and the corresponding fusion zone interstitial contamination levels. The interstitial content of the weld metal was found to be proportional to and approximately an order of magnitude less than the shielding gas composition. These results agree with those of Borland (Ref. 17). Other investigators found similar results for up to 2% nitrogen in argon, but found that nitrogen absorption in the weld metal for shielding gas compositions higher than 2% were less than those reported here (Refs. 18,

19). At the higher concentrations, it was believed that the formation of a nitrogen-rich surface layer impeded further absorption (Ref. 19).

Hardness values were obtained for the fusion zones, heat-affected zones, and base metal of all weldments in this study. The results are shown in Fig. 16. The hardness of Ti-6211 was found to be strongly dependent on oxygen or nitrogen content, with nitrogen having a slightly stronger hardening effect. This dependence is very similar to that noted in earlier work (Refs. 20, 21). Hardness readings taken in the heat-affected zone deviated very little from the base metal hardness, regardless of the level of fusion zone contamination. This indicates that the absorption of nitrogen and oxygen into the heat-affected zone is not significant.

The weldments were then subjected to Varestraint testing, using 4% augmented strain and a heat input of 40 kJ/in. (1.6 MJ/m). Although interstitial contamination has been found to induce hot cracking in other systems, no hot cracking was found (Ref. 22). However, in addition to the intergranular cracking observed in uncontaminated welds, shallow transgranular cracking was observed at the highest levels of both oxygen and nitrogen contamination. Figure 17 contrasts these transgranular cracks with the intergranular cracking described earlier. The transgranular cracking appeared to be contained within the brittle, contaminated surface layer, and occurred on too fine a scale to be quantified. The transgranular cracking was not believed to be associated with the intergranular cracking.

Figure 18 shows the results of Varestraint testing the nitrogen-contaminated weldments. Transgranular cracking was first observed at 0.175% N (0.50% N_2 in the shielding gas) and increased with the level of nitrogen contamination. The degree of intergranular fusion zone cracking increased as contamination increased up to 0.048% N (0.50% N_2 in the shielding gas), but then dropped to zero at higher nitrogen levels. The intergranular cracking in the heat-affected zone was not affected by nitrogen in the weld metal.

The results of Varestraint testing for the oxygen-contaminated welds are presented in Fig. 19. Transgranular cracking was first observed at 0.224% O (1% O_2 in the shielding gas) and increased with increasing contamination. Again, the transgranular cracking could not be quantified. The intergranular cracking in the fusion zone increased with contamination up to 0.224% O and dropped to zero at higher contamination levels, as in the nitrogen-contaminated welds. However, in these welds, heat-affected zone cracking increased significantly up to 0.224% O, and then decreased to the level found in the uncontaminated weldments.

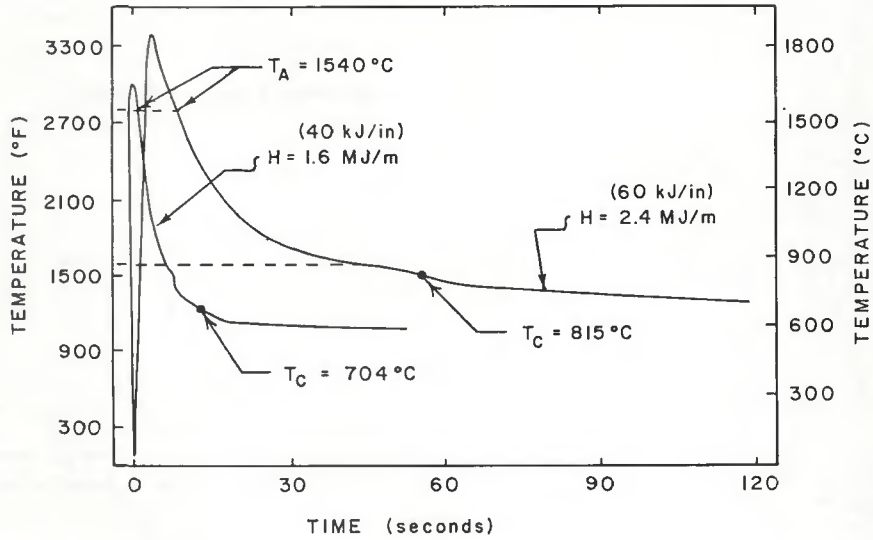

Fig. 13 — Cooling curves for weldments with two different heat inputs. The solidus and cracking temperatures are indicated

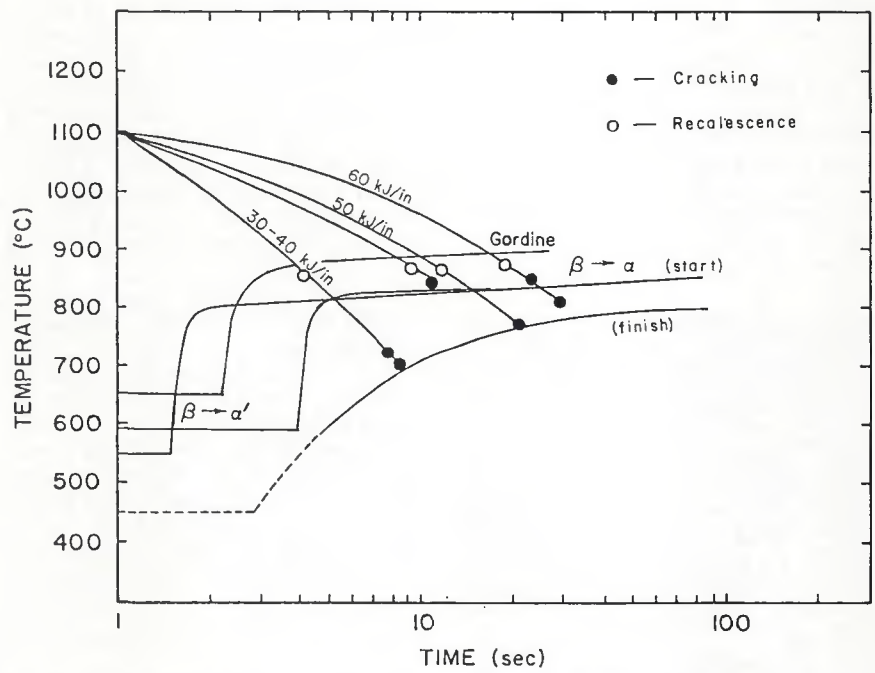

Fig. 14 — Cooling curves for several weld heat inputs superimposed on the CCT diagrams for Ti-6211 of Gordine and Damkroger (Refs. 7, 16). Note that the critical temperatures lie within the beta-to-alpha transformation

The increase in intergranular cracking with increasing oxygen or nitrogen contamination up to approximately 0.2% O or N in the weld metal is inconsistent with the differential strength model proposed by Starke, *et al.*, for the loss of elevated temperature ductility seen in some titanium alloys (Ref. 9). In this model, slip is believed to be concentrated in a weak, ductile, alpha film suspended between stronger beta grains. The slip is then believed to be blocked by a non-oriented alpha/beta interface, resulting in microvoid nucleation at this interface. Oxygen and nitrogen both partition to and strengthen the alpha phase during the transformation on cooling. Thus, this model predicts reduced cracking susceptibility with increasing oxygen or nitrogen contamination, the opposite of what was observed.

Intergranular cracking was seen to decrease at weld metal contamination levels above 0.2%. However, significant microstructural changes were observed at these contamination levels. These

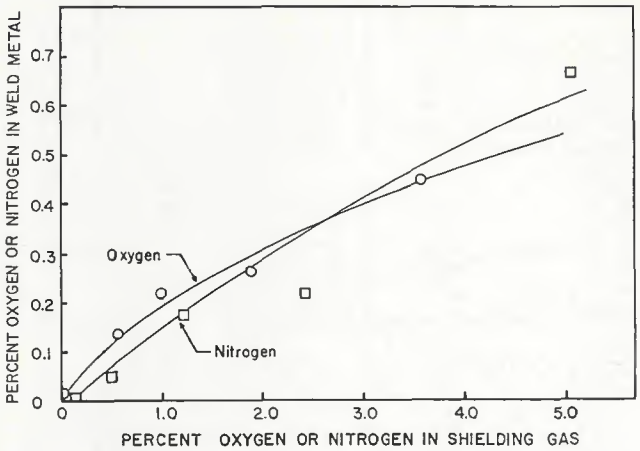

Fig. 15 — Weld metal interstitial content as a function of shielding gas content

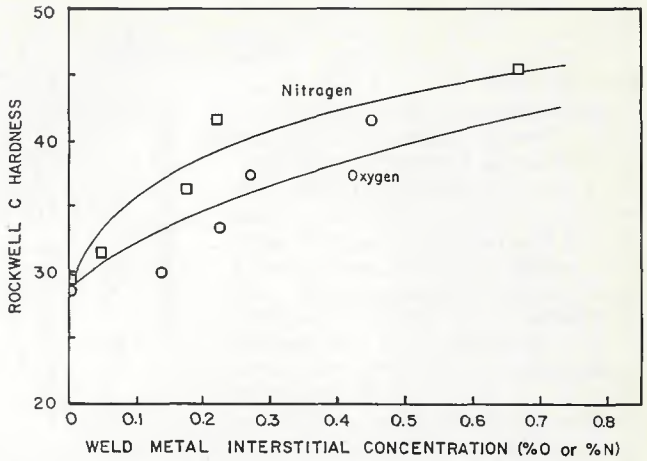

Fig. 16 — Rockwell C hardness of weld metal as a function of oxygen or nitrogen content

changes are believed to be responsible for the reduction of intergranular cracking. The change in the beta grain morphology with oxygen or nitrogen additions can be seen in Fig. 20. This figure shows macrographs of the top surfaces of contaminated and uncontaminated welds. In the uncontaminated weld, the beta grains appear equiaxed in the plane of the macrograph, and have many grain boundaries oriented perpendicular to the axis of the augmented strain. In the nitrogen-contaminated weld, the grains are narrow and elongated parallel to the weld axis. In this weld, the majority of the grain boundaries are parallel to the axis of straining. The development of the elongated grain morphology paralleled the decrease in intergranular cracking seen in the nitrogen-contaminated weldments. A similar change in grain morphology was seen in the oxygen-contaminated welds. This observation is consistent with the results of Starke, *et al.* (Ref. 9). In that study, a material with an equiaxed prior-beta grain structure was found to have low ductility when tensile tested at 1475°F (800°C).

Another significant microstructural change observed in these contaminated welds is shown in Figs. 21 and 22, micrographs of both contaminated and uncontaminated weld beads. It can be seen that the large lenticular patches characteristic of contaminant-free Ti-6211 weld metal are not present in the contaminated material, having been replaced by a finer, acicular transformation product. This is consistent with the observation that intergranular cracking susceptibility is reduced when fine acicular transformation products are present, or by a sufficiently rapid cooling rate. High levels of oxygen or nitrogen may prevent intergranular cracking susceptibility by altering the beta-to-alpha transformation kinetics. These elements may enhance alpha nucleation or slow the diffusion of the substitutional alloy elements. The same result would be obtained with an increased cooling rate, which causes the transformation to occur at a lower temperature and a higher level of undercooling. Either will promote the formation of a fine, acicular microstructure, shown to be less susceptible to Varestraint weld cracking.

Three models have been proposed to explain the high-temperature ductility losses which occur in certain titanium alloys. As discussed earlier, the observations made during this investigation are not entirely consistent with the differential strength proposed by Starke, *et al.* (Ref. 9). A second model has been proposed by Lewis and Caplan (Ref. 6). This model maintains that the intergranular failure observed occurs as a result of impurity segregation to the alpha-beta interface during the beta-to-alpha trans-

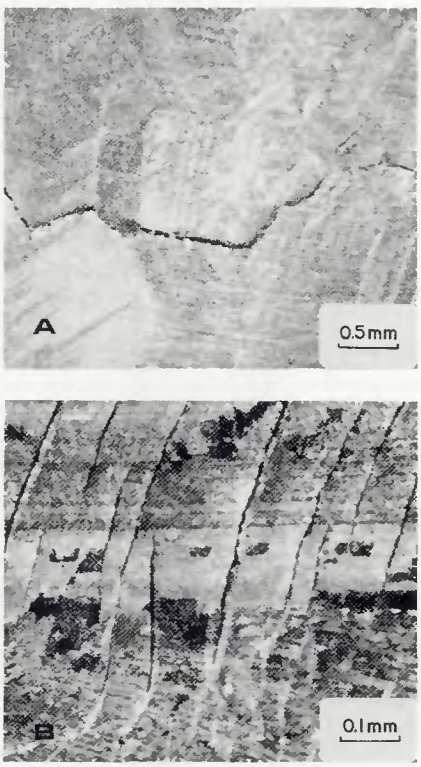

Fig. 17 — Macrographs of a nitrogen-contaminated weld contrasting — A — the intergranular cracking seen earlier, with — B — contamination-induced transgranular cracking

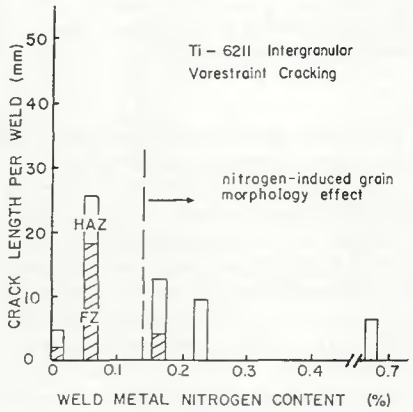

Fig. 18 — Intergranular fusion zone and heat-affected crack length as a function of weld metal nitrogen content

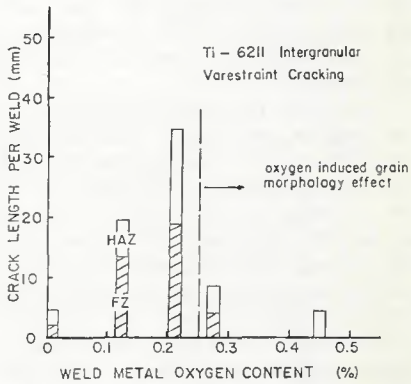

Fig. 19 — Intergranular fusion zone and heat-affected crack length as a function of weld metal oxygen content

formation. The impurity-coated interface then acts as a barrier to the transmission of slip, leading to dislocation pile-ups, stress concentration, and the nucleation of microvoids. This investigation produced no evidence either in support of, or contrary to, this model.

A third model has recently been proposed by Rath, *et al.* (Ref. 23). In this model, the stress developed due to lattice incompatibility during the beta-to-alpha transformation is believed to be related to the ductility loss. Because the initial transformation takes place at the prior-beta grain boundaries, these regions are placed in tension. The extent of this tensile stress is related to both the extent of lattice incompatibility and the extent of grain boundary transformation prior to transformation of the bulk beta grain. Therefore, this model correctly predicts that the minimum ductility temperatures in Varestraint testing would be associated with the beta-to-alpha transformation. Additionally, enhancement of intragranular nucleation would be expected to reduce the transformation stress and reduce the ductility loss susceptibility. This agrees with the observation made in this study that materials and conditions which result in a finer microstructure show a reduced cracking susceptibility.

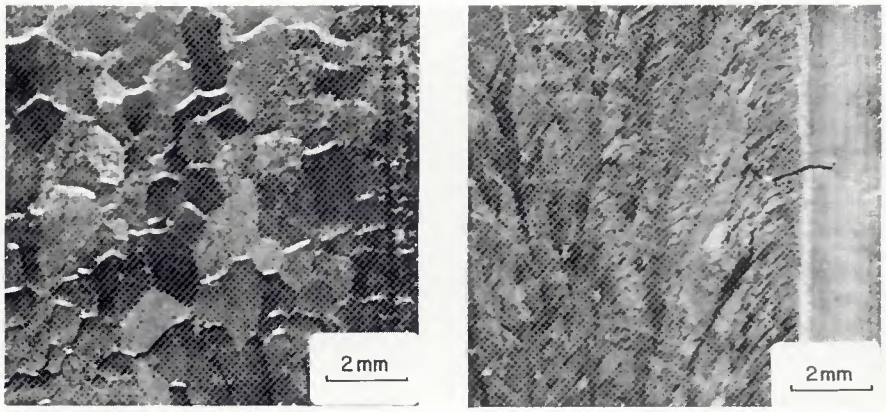

Fig. 20—Fusion zone macrographs showing the change in prior beta grain shape caused by nitrogen contamination

The weld cracking susceptibility of Ti-6211, as determined by the Varestraint test, was metallurgically characterized in this investigation. The results suggest that the Varestraint weld cracking observed in this investigation and the high-temperature ductility losses studied in earlier work (Refs. 6, 7, 9) are different manifestations of the same phenomenon. The observations made in this investigation have been evaluated with respect to two existing models for the high-temperature ductility losses. Although both the differential strength model (Ref. 9) and the lattice incompatibility model (Ref. 23) explain many of the observations made, the differential strength model is contradicted by the results of the interstitial contamination testing.

Conclusions

1. Susceptibility to weld cracking, as determined by the Varestraint test, is a function of alloy content. Ti-6Al-2Nb-1Ta-0.8Mo is more susceptible to weld

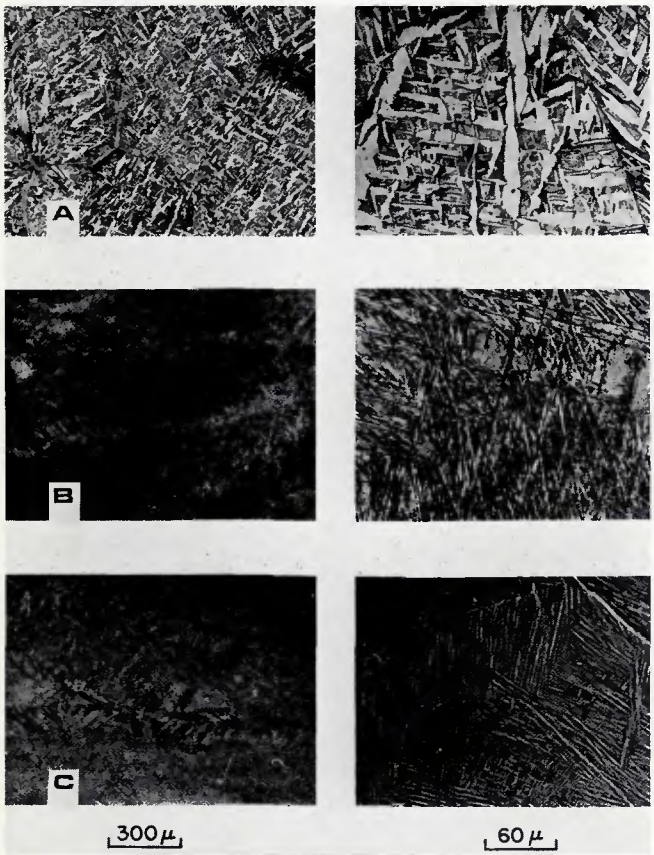

Fig. 21—Optical micrographs showing the microstructural refinement, and elimination of the large lenticular patches, caused by nitrogen contamination. A—uncontaminated; B—0.18% nitrogen; C—0.67% nitrogen

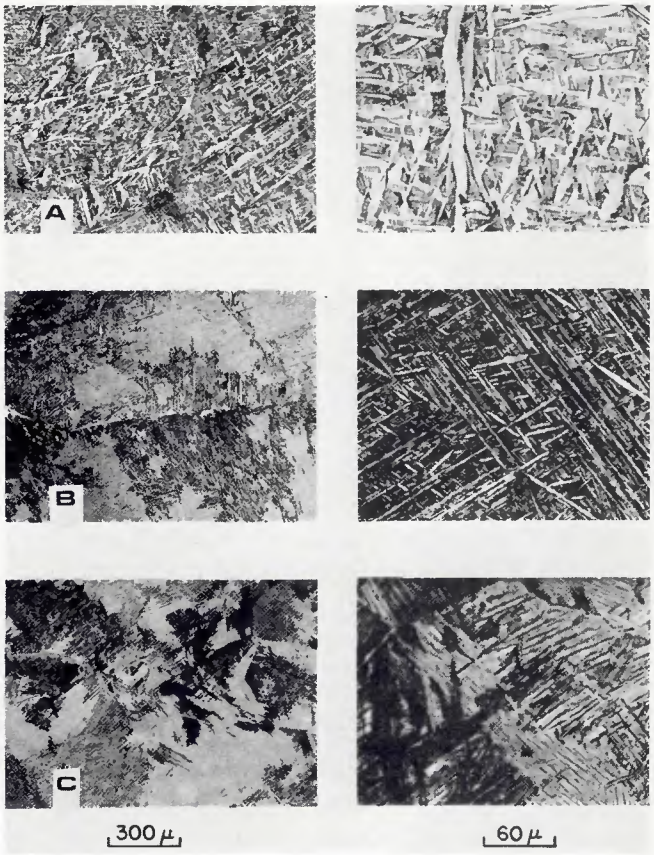

Fig. 22—Optical micrographs showing the microstructural changes and refinement which are induced by oxygen contamination. A—uncontaminated; B—0.27% oxygen; C—0.45% oxygen

cracking than Ti-6Al-4V and other titanium alloys.

2. Parallel observations between this work and the work of other investigators suggest that the Varestraint weldment cracking in Ti-6211 and the reported hot ductility dip in Ti-6211 are different manifestations of the same phenomenon.

3. The Varestraint weld cracking is associated with a critical temperature range which is within the beta-to-alpha transformation. Alterations of the beta-to-alpha transformation kinetics, which result in a refined microstructure, reduce the weld cracking susceptibility. These observations suggest that the mechanism of cracking is tied to the transformation.

4. The cracking susceptibility of Ti-6211 is enhanced by oxygen and nitrogen additions to the weld metal. This contradicts the existing "differential strength" model, which maintains that strain concentration in the alpha phase is responsible for this cracking.

Acknowledgments

This work was sponsored by the Office of Naval Research under Contract No. N00014-80-C-0607, Dr. Bruce A. MacDonald, Program Manager, and was conducted at the Center for Welding Research at the Colorado School of Mines.

References

1. Scott, M. H. 1979. Arc welding titanium. *Welding Institute Research Bulletin*, pp. 163–168.

2. Savage, W. F., and Lundin, C. D. 1968. The evaluation of the weldability of structural alloys with the Varestraint test. Technical Report AFML-TR-68-48. Wright-Patterson Air Force Base, Dayton, Ohio, Air Force Materials Laboratory, Air Force Systems Command.

3. Baeslack, W. A., III. 1968. Observations of solidification cracking in Ti alloy weldments. *Metallography* 13:277–281.

4. Becker, D. W., Messler, R. W., Jr., and Baeslack, W. A., III. 1980. Titanium welding: a critical review. *Titanium '80 Science and Technology Proceedings of the Fourth International Conference on Titanium*, eds. H. Kimura and O. Izumi, pp. 255–276, Warrendale, Pa., TMS/AIME.

5. Shull, R. D. Private communication, Washington, D.C., National Bureau of Standards.

6. Lewis, R. E. 1978. Technical report LMSC-D623740. Palo Alto, Calif., Lockheed Missiles and Space Co.

7. Hayduk, D., Damkroger, B. K., Edwards, G. R., Olson, D. L., and Matlock, D. K. 1983. Titanium welding metallurgy: cracking susceptibility. Golden, Colo., The Center for Welding Research. Unpublished research.

8. Misra, M. Private communication, Denver, Colo., Martin Marietta Aerospace Co.

9. Bowden, D. M., and Starke, E. A., Jr. 1984. Effect of microstructures and deformation behavior on the hot ductility of Ti-6211. *Metallurgical Transactions A* 15A (9):1687–1698.

10. Inouye, H., and David, S. 1984. Segregation and influence of boron on the impact toughness of Ti-6211 welds and castings. *Metallurgical Transactions A* 15A (7):1505–1507.

11. Savage, W. F., and Lundin, C. D. 1965. The Varestraint test. *Welding Journal* 44 (10):433-s to 442-s.

12. Gould, J. E., Becker, D., and Williams, J. C. 1980. Microstructural characterization of Ti weldments. *Physical Metallurgy of Metal Joining, TMS/AIME Conference Proceedings*, eds. R. Kossowsky and M. E. Glicksman, pp. 199–221. Warrendale, Pa., TMS/AIME.

13. Savage, W. F., and Lundin, C. D. 1966. Application of the Varestraint technique to the study of weldability. *Welding Journal* 45 (11):497-s to 503-s.

14. Lewis, R. E., *et al.* 1981. Continuous cooling transformations in Ti-6Al-2Cb-1Ta-0.8Mo. *Solid-Solid Phase Transformations, TMS/AIME Conference Proceedings*, eds. H. I. Aaronson, D. E. Laughlin, R. E. Sekerka, and C. M. Wayman, pp. 1499–1503, Warrendale, Pa., TMS/AIME.

15. Adams, C. M. 1958. Cooling rates and peak temperatures in fusion welding. *Welding Journal* 37 (5):210-s to 215-s.

16. Gordine, J. 1974. Weld heat-affected zones in Titanium-6Al-2Cb-1Ta-1Mo. *Welding Journal* 53 (3):117-s to 124-s.

17. Borland, J. C. 1961. Effect of oxygen and nitrogen on properties of welds in unalloyed titanium. *British Welding Journal* 8 (2):61–67.

18. Demyantsev, V. P., and Matyukhin, V. I. 1975. Special features of the absorption of nitrogen by molten titanium in welding with an immersed arc using a non-consumable electrode. *Svar. Proiz.* 7:1–3.

19. Murav'ev, I. I., and Gorshkov, A. I. 1976. The effect of the purity of argon on the content of gas impurities in the weld metal of titanium welded in chambers. *Svar. Proiz.* 6:26–27.

20. Barrett, J. C., and Lane, I. R., Jr. 1954. Effect of atmospheric contaminants on arc welds in titanium. *Welding Journal* 33 (3):121-s to 128-s.

21. McKinley, T. D. 1956. Effect of impurities on the hardness of titanium. *Journal of The Electrochemical Society* 103:561–567.

22. Cieslak, M. J., Ritter, A. M., and Savage, W. F. 1982. Solidification cracking and analytical electron microscopy of austenitic stainless steel weld metals. *Welding Journal* 61 (1):1-s to 8-s.

23. Damkroger, B. K., Rath, B. B., Imam, M. A., and Edwards, G. R. 1985. A model for high-temperature ductility losses in titanium alloys. Submitted to *Metallurgical Transactions A*.

WRC Bulletin 314
May 1986

Bolted Flanged Connections with Full Face Gaskets
By A. E. Blach, A. Bazergui and R. Baldur

A flange type commonly called "flat-face" flange has been used in certain classes of bolted flanged connections for many years, yet no code rules exist to cover this class of flanged connections. This paper analyzes the behavior of gaskets and flanges in such a connection and gives design formulas which follow the philosophy of the present code rules for bolted flanged connections. A numerical example is included which shows the application of the design formulas and compares results obtained with values from strain gage measurements on a pressure vessel of the same size.

Publication of this report was sponsored by the Subcommittee on Bolted Flanged Connections of the Pressure Vessel Research Committee of the Welding Research Council. The price of WRC Bulletin 314 is $12.00 per copy, plus $5.00 for postage and handling. Orders should be sent with payment to the Welding Research Council, Ste. 1301, 345 E. 47th St., New York, NY 10017.